Structural basis for CDK6 activation by a virus-encoded cyclin

Ursula Schulze-Gahmen[1] and Sung-Hou Kim[1,2]

[1]*Physical Bioscience Division at E. O. Lawrence Berkeley National Laboratory, and* [2]*Department of Chemistry, University of California Berkeley, California 94720, USA*

Published online: 4 February 2002, DOI: 10.1038/nsb756

Cyclin from herpesvirus saimiri (Vcyclin) preferentially forms complexes with cyclin-dependent kinase 6 (CDK6) from primate host cells. These complexes show higher kinase activity than host cell CDKs in complex with cellular cyclins and are resistant to cyclin-dependent inhibitory proteins (CDKIs). The crystal structure of human CDK6–Vcyclin in an active state was determined to 3.1 Å resolution to better understand the structural basis of CDK6 activation by viral cyclins. The unphosphorylated CDK6 in complex with Vcyclin has many features characteristic of cyclinA-activated, phosphorylated CDK2. There are, however, differences in the conformation at the tip of the T-loop and its interactions with Vcyclin. Residues in the N-terminal extension of Vcyclin wrap around the tip of the CDK6 T-loop and form a short β-sheet with the T-loop backbone. These interactions lead to a 20% larger buried surface in the CDK6–Vcyclin interface than in the CDK2–cyclinA complex and are probably largely responsible for the specificity of Vcyclin for CDK6 and resistance of the complex to inhibition by INK-type CDKIs.

The mammalian cell cycle consists of four stages: S phase (S), where DNA synthesis occurs; mitosis (M), when the actual cell division takes place; and two gap phases (G1 and G2), during which required cell components are replicated. The progression of cells through G1 phase and the G1/S transition is regulated by complexes of the cyclin-dependent kinases 4/6 (CDK4/6) with cyclinD and CDK2 with cyclinE[1]. Mitogen-induced signaling activates CDK4/6 by up-regulating levels of their cyclinD activators[2], which promotes the expression of other cyclins. Inactive CDK apoenzymes are partially activated by complex formation with regulatory cyclin subunits. The CDK–cyclin complexes are further activated by phosphorylation of a Thr residue (Thr 160 in CDK2) in the activation loop (T-loop), which spans residues Asp 145^{CDK2} (the DFG motif)–Glu 172^{CDK2} (the APE motif). DFG and APE motifs are conserved sequences between protein kinases, such as cAPK, CDKs, ERK and Src, that are found at the ends of the activation loops in all of the kinases. CDK activity is also regulated by complex formation with cyclin-dependent inhibitory proteins (CDKIs) of the CIP/KIP and INK type[3].

Deregulation of the G1/S transition point is a common event in tumorigenesis[4,5]. Several viruses that are able to transform cells are known to encode an open reading frame with cyclin homology in their genomes[6]. The two best characterized virus-encoded cyclins, from herpesvirus saimiri[7] and Kaposi's sarcoma herpesvirus[8,9], have homology closest to human D-type cyclins and preferentially activate CDK6. These CDK6 complexes show higher kinase activity than CDK complexes with cellular cyclins, are resistant to cyclin-dependent inhibitory proteins of the CIP/KIP- and INK-types[10] and can phosphorylate retinoblastoma protein as well as histone H1. To address questions concerning the active form of CDK6, the specificity of cyclins for different CDKs, and the unique structural and functional characteristics of viral cyclins, we determined the 3.1 Å resolution structure of human CDK6 in complex with a virus-encoded cyclin (Vcyclin) from herpesvirus saimiri.

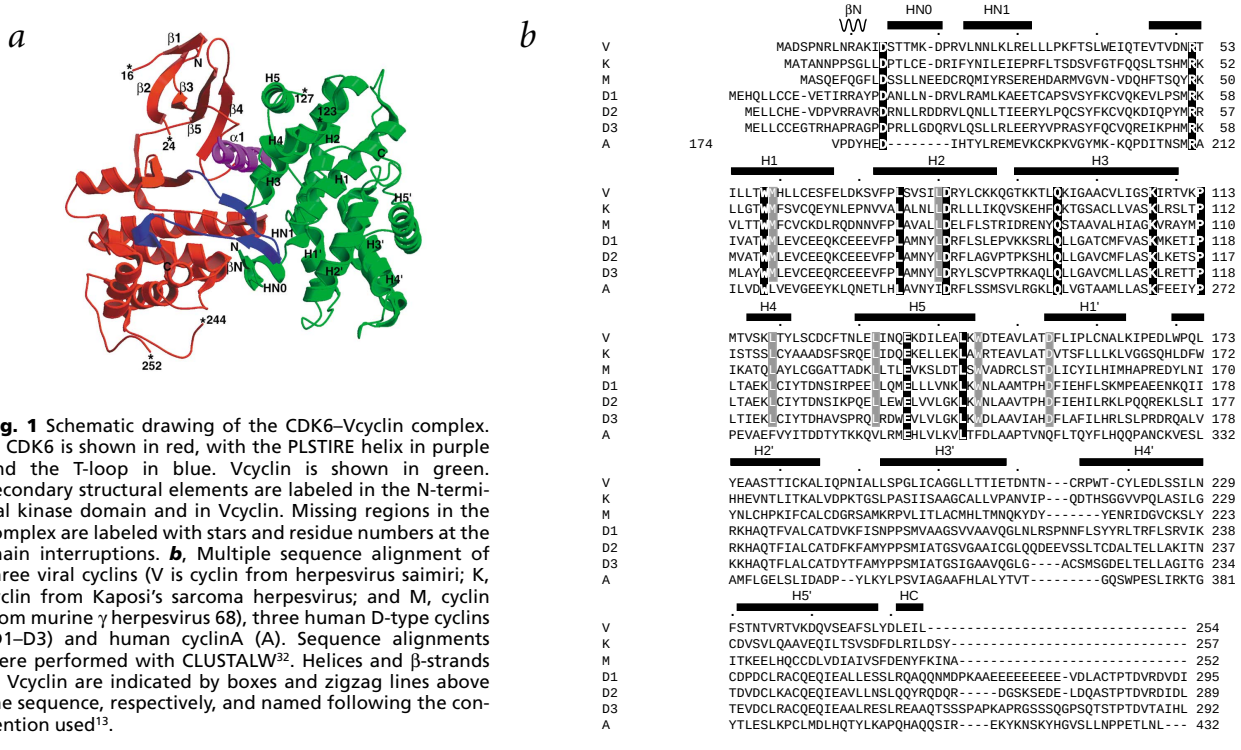

Fig. 1 Schematic drawing of the CDK6–Vcyclin complex. ***a***, CDK6 is shown in red, with the PLSTIRE helix in purple and the T-loop in blue. Vcyclin is shown in green. Secondary structural elements are labeled in the N-terminal kinase domain and in Vcyclin. Missing regions in the complex are labeled with stars and residue numbers at the chain interruptions. ***b***, Multiple sequence alignment of three viral cyclins (V is cyclin from herpesvirus saimiri; K, cyclin from Kaposi's sarcoma herpesvirus; and M, cyclin from murine γ herpesvirus 68), three human D-type cyclins (D1–D3) and human cyclinA (A). Sequence alignments were performed with CLUSTALW[32]. Helices and β-strands in Vcyclin are indicated by boxes and zigzag lines above the sequence, respectively, and named following the convention used[13].

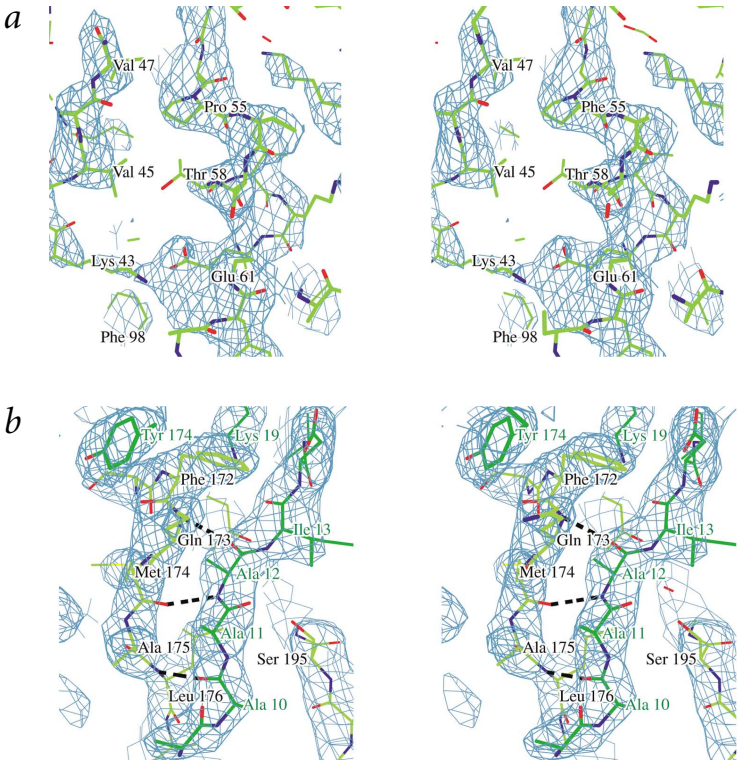

Fig. 2 Electron density maps for the CDK6–Vcyclin complex. ***a***, A simulated-annealing omit map was calculated for an 8 Å sphere around Thr 58 in the N-terminal CDK6 domain. The α_{calc} ($|F_o| - |F_c|$) Fourier map was calculated at 3.1 Å resolution with SIGMAA-weighted[33] coefficients and contoured at 2.4 σ. ***b***, The α_{calc} ($2|F_o| - |F_c|$) Fourier synthesis was calculated at 3.1 Å resolution with SIGMAA-weighted[33] coefficients for part of the CDK6 T-loop (light green model with black labels) and the N-terminal β-strand of Vcyclin (dark green model with green labels). The map is contoured at 1.4 σ. Backbone hydrogen bonds between the β-strands from CDK6 and Vcyclin are drawn as broken lines.

Overall structure of the complex

CDK6 in complex with Vcyclin is comprised of an N-terminal and C-terminal lobe, with the ATP-binding pocket and catalytic site located between the two lobes (Fig. 1*a*). The N-terminal lobe has a higher average B-factor (85 Å^2) than the rest of the structure, with parts of strand β1 undefined in the electron density. However, elements located close to the CDK–cyclin interface, such as the PLSTIRE helix (α1) and strand β4, are well defined in the electron density map (Fig. 2*a*). The unphosphorylated T-loop in the C-terminal domain, which contains the potential phosphorylation site Thr 177^{CDK6}, is also well ordered in this structure, in contrast to the T-loop in other unphosphorylated CDKs[11,12]. The Vcyclin subunit consists of two domains, each adopting the typical cyclin fold (Fig.1*a*,*b*), and an N-terminal extension with a β-sheet (βN) and two N-terminal helices (HN0 and HN1). Residues in the N-terminal β-sheet and helix HN0 were disordered in the crystal structure of Vcyclin alone[13]. In the complex with CDK6, these residues wrap around the T-loop and form stable secondary structures (Fig. 2*b*). There are no homologous contacts in other CDK2–cyclin complexes[12,14–16], even though the N-terminal extension in the cyclin from murine γ herpesvirus (Mcyclin) also interfaces the T-loop and is essential for CDK2 activation by Mcyclin[15].

Structural comparison of CDK6 from the Vcyclin complex with kinase domains in complexes of CDK2 with cyclinA[14], Mcyclin[15] or the free apoenzyme[11], and in CDK6–inhibitor complexes[16–18] identified the phosphorylated CDK2–cyclinA complex as the structure with the highest similarity. The phosphorylated CDK2–cyclinA complex has 123 equivalent residues in the C-terminal kinase domain and 43 equivalent residues in the N-terminal kinase domain, with root mean square (r.m.s.) deviations on Cα atoms of 0.52 and 0.85 Å, respectively, and small differences in relative domain orientations of ~15°. In addition, Vcyclin and cyclinA bind CDK in similar orientations relative to the critical α1 helix, which is central to the activation of CDKs, and the T-loop (Fig.3*a*). Although Vcyclin binding to CDK6 induces an active kinase conformation similar to that found in phosphorylated CDK2, the intermolecular contacts between kinase and cyclin show some significant differences, implicating some differences in the activation mechanism of CDK6 by Vcyclin compared to that of CDK2 by cyclinA.

Structure of the CDK6–Vcyclin interface

The CDK6–Vcyclin interface can be divided into two parts: an area that involves contacts with the α1 helix and another area that involves contacts with the T-loop region of CDK6. The CDK6–Vcyclin complex shows the same rotational and translational shift of α1 into the catalytic cleft as the CDK2–cyclinA complex, leading to the conservation of hydrogen bonds between Vcyclin residues Lys 107^{Vcyc} and Glu 136^{Vcyc} and backbone atoms of Glu 52^{CDK6} and Met 54^{CDK6}, and conserved hydrogen bonds involving Arg 60^{CDK6} and Arg 66^{CDK6}, respectively (Table 1). Six of the nine hydrogen bonds and salt bridges with residues in the PLSTIRE region are conserved between the CDK6–Vcyclin and CDK2–cyclinA complexes. The shift of the α1 helix during CDK activation causes the reorientation of Glu 61^{CDK6} into the binding cleft, where it is in the vicinity of Lys 43^{CDK6} and Asp 163^{CDK6}. These three residues form a triad of catalytic residues conserved in all eukaryotic kinases. They are involved in ATP phosphate orientation and Mg^{2+} coordination[12].

The buried surface area of ~1,070 Å^2 between the CDK6 T-loop and Vcyclin makes up one-third of the total 3,290 Å^2 of buried surface area. In comparison, the total buried surface area in the phosphorylated CDK2–cyclinA complex is 2,700 Å^2, of which 650 Å^2 can be attributed to T-loop contacts. Therefore, two-thirds of the differences in total buried surface area between CDK2–cyclinA and CDK6–Vcyclin are due to differences in the buried T-loop surface. The T-loops in both complexes form similar contacts with residues at the C-terminal end of helix H3 and the H3–H4 loop of the cyclin. However, residues in the N-terminal helix of cyclinA merely contact the tip of the T-loop in CDK2, whereas residues in HN0 and βN of Vcyclin wrap around the T-loop and form an antiparallel β-sheet with the T-loop region (Fig. 3*a*,*c*). A large number of van der Waals contacts and five hydrogen bonds between the backbone atoms of the N-terminal β-strand in Vcyclin and T-loop residues in CDK6 (Table 1) lock the activation loop in a stable conformation that, in the T-loop stem region, is similar to the conformation of the phosphorylated CDK2.

Only residues 172^{CDK6}–177^{CDK6} at the tip of the T-loop adopt a different conformation in CDK6 than CDK2. Residues 171–174

in CDK6 adopt a classical type II turn conformation, whereas the corresponding residues, 153–155, in CDK2 form an unclassified type of bend. The loop in CDK6 is one residue shorter than the one in CDK2 and extends further out towards domain 2 of Vcyclin. Simultaneously, a slightly different tilt of helix H2′ in Vcyclin (Fig. 3*a*) allows residues Trp 170^{Vcyc}, Pro 171^{Vcyc} and Tyr 174^{Vcyc} to form contacts with T-loop residues, in particular Phe 172^{CDK6}. Phe 172^{CDK6}, which becomes almost completely buried between hydrophobic residues from helices HN0, H1′ and H2′ of Vcyclin (Fig. 3*c*), contributes the largest buried surface of any single CDK6 residue (111 Å^2) to the CDK6–Vcyclin interface. Equivalent residues in the CDK2 T-loop are much less buried in the cyclinA or Mcyclin complexes and lack contacts with helix H2′ of the cyclin.

T-loop conformation and substrate binding

In the inactive CDK2 apoenzyme, the T-loop blocks access to the catalytic site between the two kinase domains. CyclinA binding to CDK2 relieves the steric block at the entrance of the catalytic cleft, but only phosphorylation of Thr 160^{CDK2} (Thr 177 in CDK6) induces the fully active T-loop conformation. This state is characterized by a network of hydrogen bonds between the phosphate group on Thr 160^{CDK2} and Arg residues from the α1 helix, the catalytic loop and the T-loop[14]. The Thr 160 phosphate group organizes and stabilizes the active CDK2 conformation and contributes to substrate binding of a basic residue in the P+3 position (third residue after a Ser or Thr residue in a consensus substrate sequence for CDK)[19]. Val 164^{CDK2} in phosphorylated CDK2 adopts an unusual left-handed conformation, thereby forming a specific binding pocket for a Pro residue in the P+1 position of the kinase substrates[19].

The conformation of the activation loop (residues 163–189) in the unphosphorylated CDK6–Vcyclin complex is very similar to that of the phosphorylated CDK2–cyclinA complex, with r.m.s. values of 0.67 and 0.65 Å for the Cα atoms of residues 163^{CDK6}–171^{CDK6} and 179^{CDK6}–189^{CDK6}, respectively, in the two loop stems (Fig. 3*b*). The homologous Arg residues 60, 144 and 168 from the α1 helix, the catalytic loop and the T-loop in the unphosphorylated CDK6 adopt very similar conformations as in the phosphorylated CDK2. The guanidinium groups form hydrogen bonds with backbone carbonyl oxygens in the T-loop and with the hydroxyl group of the Tyr 196^{CDK6} side chain. They are positioned closely to the C-terminal end of helix H3 in Vcyclin, forming several hydrogen bonds with the carbonyl oxygens of the last helical turn (residues 107^{Vcyc}–110^{Vcyc}). The helical dipole moment[20] gives the C-terminal end of the α-helix a partial negative charge that will balance the cluster of positive charges from the Arg residues (Fig. 3*b*).

Val 181^{CDK6} in the CDK6–Vcyclin complex adopts the same left-handed conformation as Val 164 in phosphorylated CDK2, which is necessary to form a substrate binding pocket for the minimal consensus CDK substrate sequence — that is, a Ser or Thr followed by a Pro residue. The substrate specificity of the CDK6–Vcyclin complex for the P+3 substrate position is unknown. However, studies on the substrate preference of CDK4/6 complexes indicate a less stringent requirement for a basic residue in the P+3 position[21,22]. Considering that CDK6 complexes with viral cyclins possess high specific kinase activity in the unphosphorylated, as well as phosphorylated form[16] (unpublished results), and that the phosphorylated Thr residue in the T-loop contributes to substrate specificity in CDK2, CDK6 in complex with viral cyclins could conceivably have different substrate specificities depending on the phosphorylation state.

Table 1 Hydrogen bonds at the CDK6–Vcyclin and CDK2–cyclinA interface[1]

CDK6	Vcyclin	CDK2	CyclinA
		E40[2]	K289[2]
		t41	K288
E52	v116		
E52	**K107**	**e42**	**K266**
m54	**K107**	**v44**	**K266**
m54	**E136**	**v44**	**E295**
R60 (2)[3]	k107		
R60	**i108**	**R50 (2)**	**f267**
R60	t110		
R66	**k144**	**K56**	**t303**
R66[2]	**D146**[2]	**K56**[2]	**D305**[2]
		E57	Y185
		t72	H296
H139	N26		
R140[2]	D154[2]	R122 (2)	a307
R168	**i108**	**R150 (2)**	**e268**
		R150[2]	E268[2]
Y170 (2)	i13		
		v154	t316
		v154	q317
q173	a12		
m174	a12		
		R157[2]	E268[2]
a175	D69		
l176	a10		
T198	S15		
		k278	Y178
		K278[2]	D181[2]

[1]Upper case letters indicate side chain contacts, lower case letters main chain contacts. Conserved hydrogen bonds between CDK6 and CDK2 complexes are highlighted in bold letters. A distance criterion of 3.4 Å was used.
[2]Salt bridge.
[3]Numbers in parentheses indicate multiple hydrogen bonds with one residue.

CDK–cyclin specificity

Different cyclins preferentially form complexes with different CDKs *in vivo*. These preferences may be due to spatial and temporal accumulation of certain cyclins and CDKs in parts of the cell during cell cycle progression. In addition, certain complex formations may be preferred, based on energetically more or less favorable subunit interactions. *In vitro* studies on complexes between ectopically expressed Vcyclin and CDKs in COS cells showed that Vcyclin almost exclusively associates with CDK6 (ref. 7).

Analysis of a CDK2–Vcyclin model complex, which was constructed by superimposing the N-terminal domain of Vcyclin onto cyclinA in the CDK2 complex, identified one major area with many unfavorably close contacts between the N-terminal extension (residues 10–20) in Vcyclin and the T-loop in CDK2. In the CDK6–Vcyclin complex, the tip of the CDK6 T-loop is deeply buried between residues in helices H1′, H2′ and the N-terminal extension in Vcyclin (Fig. 3*c*). If Vcyclin would bind to CDK2 in the same conformation, residues in the N-terminal extension would overlap with residues in the CDK2 T-loop, as well as with residues Lys 178^{CDK2} and Tyr 179^{CDK2} in a loop N-terminal to helix α4 (Fig. 3*c*). CDK6 has a one-residue deletion and smaller side chains in the corresponding loop, which leaves room for residues in βN of Vcyclin. Vcyclin would be able

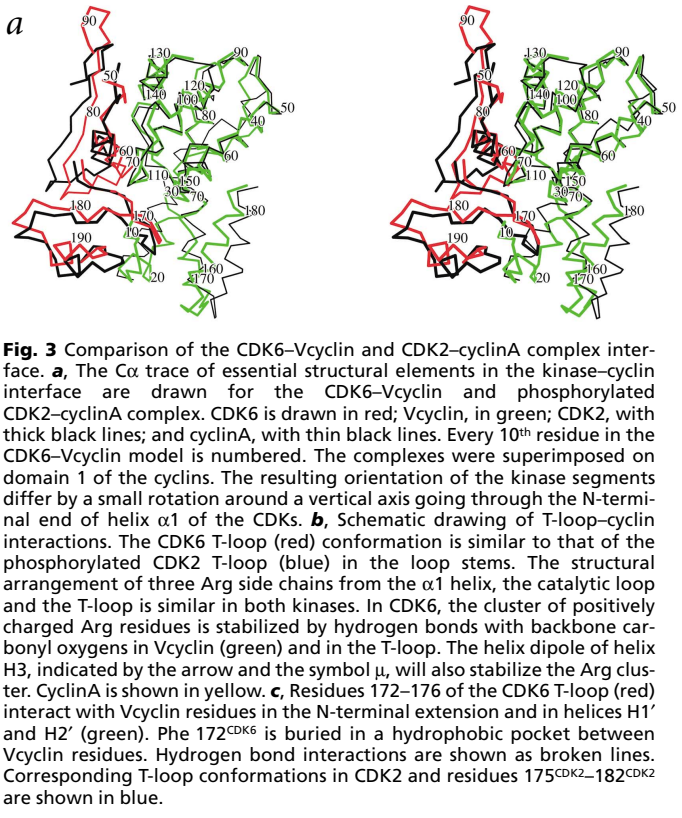

Fig. 3 Comparison of the CDK6–Vcyclin and CDK2–cyclinA complex interface. ***a***, The Cα trace of essential structural elements in the kinase–cyclin interface are drawn for the CDK6–Vcyclin and phosphorylated CDK2–cyclinA complex. CDK6 is drawn in red; Vcyclin, in green; CDK2, with thick black lines; and cyclinA, with thin black lines. Every 10th residue in the CDK6–Vcyclin model is numbered. The complexes were superimposed on domain 1 of the cyclins. The resulting orientation of the kinase segments differ by a small rotation around a vertical axis going through the N-terminal end of helix α1 of the CDKs. ***b***, Schematic drawing of T-loop–cyclin interactions. The CDK6 T-loop (red) conformation is similar to that of the phosphorylated CDK2 T-loop (blue) in the loop stems. The structural arrangement of three Arg side chains from the α1 helix, the catalytic loop and the T-loop is similar in both kinases. In CDK6, the cluster of positively charged Arg residues is stabilized by hydrogen bonds with backbone carbonyl oxygens in Vcyclin (green) and in the T-loop. The helix dipole of helix H3, indicated by the arrow and the symbol μ, will also stabilize the Arg cluster. CyclinA is shown in yellow. ***c***, Residues 172–176 of the CDK6 T-loop (red) interact with Vcyclin residues in the N-terminal extension and in helices H1′ and H2′ (green). Phe 172^{CDK6} is buried in a hydrophobic pocket between Vcyclin residues. Hydrogen bond interactions are shown as broken lines. Corresponding T-loop conformations in CDK2 and residues 175^{CDK2}–182^{CDK2} are shown in blue.

to bind to CDK2 only after major conformational changes in Vcyclin or CDK2.

CDKI resistance

The CDK6–Vcyclin complex is resistant to inhibition by CDKIs of KIP and INK type[3,10]. The binding pocket for residues 25–32 in the $p27^{KIP1}$-coil region on the cyclinA subunit[23] is formed mostly by helix H1, at the bottom of the pocket, and loop H4–H5, which is on one side of the bound inhibitor segment. The equivalent binding pocket in Vcyclin and Mcyclin is narrower due to a short C-terminal helix that is positioned close to the p27-binding pocket. Residues in the C-terminal helix of Vcyclin would make unfavorably close contacts, especially with Arg 30^{KIP1}, in a model inhibitor complex. The H4–H5 loop is disordered in Vcyclin and adopts different conformations in other viral cyclin structures[15,16]. The sequence for this loop is conserved between cellular cyclins but without homologies in the viral cyclins (Fig. 1*b*). The H4–H5 loop provides a salt bridge interaction between Asp 283^{CycA} and Lys 25 ^{KIP1} that is missing in the viral cyclins. In addition, side chain replacements at the C-terminal end of H1 in all viral cyclins eliminate an important hydrogen bond and a salt bridge between Glu 220^{CycA} and residues Ser 27 and Arg 30 from $p27^{KIP1}$ (Fig. 1*b*). Hence, single side chain replacements, as well as steric obstructions by C-terminal residues in viral cyclins, may prevent p27 binding to the viral cyclin subunits.

Inhibitors of the INK family bind to CDK6 opposite the cyclin-binding site[16–18]. Resistance of the CDK6–Vcyclin complex to INK-type inhibitors may be restricted to the phosphorylated form of the complex, which was recently shown for the homologous CDK6–Kcyclin (cyclin from Kaposi's sarcoma herpesvirus) complex[16]. INK-type inhibitors induce structural changes in the kinase that distort the catalytic cleft, interfere with ATP binding and propagate to the cyclin binding site. The CDK–cyclin interface in the CDK6–Vcyclin complex is 20% larger than in the CDK2–cyclinA complex. The additional contacts between CDK6 T-loop and the Vcyclin N-terminal extension may stabilize the active kinase conformation and shift the equilibrium away from the $p16^{INK4}$-induced distorted inactive conformation. If phosphorylation of the T-loop Thr residue also contributes to stabilization of the active kinase conformation[14], the phosphorylated CDK complexes with viral cyclin would be expected to be more resistant to INK-type inhibitors than unphosphorylated CDK complexes.

Conclusions

The crystal structure of CDK6–Vcyclin shows highest similarity to the phosphorylated CDK2–cyclinA complex. The PLSTIRE helix is moved into the catalytic cleft, resulting in the productive alignment of critical catalytic residues. The T-loop stem conformation and a cluster of three Arg side chains is similar to that observed in the phosphorylated active CDK2. Val 181^{CDK6} in the T-loop adopts a left-handed conformation necessary to form a functional substrate binding pocket. These structural homologies confirm essential features for CDK activation in general. The CDK6–Vcyclin complex shows, however, differences in the conformation of the tip of the T-loop and its interactions with Vcyclin. N-terminal Vcyclin residues outside the conserved cyclin fold wrap around the tip of the CDK6 T-loop, forming a short β-sheet with the T-loop and burying CDK6 side chains at the tip of the loop. These interactions lead to a 20% larger buried surface in the CDK6–Vcyclin interface and probably contribute to Vcyclin specificity for CDK6. They may also more effectively stabilize the active kinase confomation, making the enzyme resistant to inhibition by INK-type CDKIs.

Table 2 Crystallographic results

Data collection	
Resolution (Å)	30.0–3.1
Total observations	92,567
Unique reflections	12,678
Completeness (%)[1]	97.9 (81.8)
Mean I / σ_I[1]	29.1 (4.0)
R_{sym} (%)[1,2]	5.8 (29.0)
Refinement	
Resolution (Å)	20.0–3.1
Data/parameter	0.8
R_{cryst} / R_{free}[3]	0.266 / 0.323
R.m.s. deviations	
Bonds (Å)	0.008
Angles (°)	1.50
Ramachandran analysis (%)	
Most favored Φ / Ψ[4]	75.1
Allowed	23.2
Disallowed	1.7
Average B-factor (Å^2)[5]	70

[1]The number in parentheses is for the outer shell.
[2]$R_{sym} = \Sigma_{hkl} \Sigma_i |I - \langle I \rangle| / \Sigma_{hkl} \Sigma_I$.
[3]$R_{cryst} = \Sigma_h ||F_o(h)| - |F_c(h)|| / \Sigma_h |F_o(h)|$ for all data, R_{free} was calculated from 7.5% of structure factor amplitudes that were excluded from refinement.
[4]Most favored region in Ramachandran plot as defined in PROCHECK[26].
[5]One B-factor per residue.

Methods

Protein expression, crystallization and data collection. Protein expression, purification, crystallization and data collection have been reported[24]. Data to 3.1 Å from one cryo-cooled crystal were collected at the Advanced Light Source (Lawrence Berkeley National Laboratory) beamline 5.02 and processed with the HKL package[25]. Autoindexing and examination of systematic absences indicated that the space group is $P6_122$ or $P6_522$, with unit cell parameters a = b = 70.14 Å, c = 448.77 Å, γ = 120° and one complex per asymmetric unit. The overall B-factor for diffraction data from the Wilson plot is 68.1 Å^2.

Structure determination and model refinement. The structure of the CDK6–Vcyclin complex was solved by molecular replacement. A model of the free Vcyclin[13] was placed in the asymmetric unit using AmoRe[26]. This solution clearly identified the space group as $P6_522$. However, attempts to place the kinase domains by molecular replacements methods using CDK6 and CDK2 as models were unsuccessful. Hence, an initial model for the complex was constructed by superimposing cyclinA from the CDK2–cyclinA complex onto the Vcyclin solution. The resulting CDK2–Vcyclin complex was then submitted to rigid body refinement followed by replacement of CDK2 domains by the corresponding CDK6 domains. Parts of the kinase structure that might show structural differences were omitted from the initial model, which consisted of the full length Vcyclin; the N-terminal kinase domain segments 39–44, 73–84 and 94–100 with side chains truncated to Ala; and the C-terminal kinase domain without T-loop. The model was refined using CNS[27] and manual fit in O[28] to a final R-value of 26.6% (R_{free} = 32.3%) at 3.1 Å (Table 2). In the course of refinement, most of the omitted regions could be traced. The final structure has undefined density for residues 1–8 and 124–126 in Vcyclin and residues 1–9, 17–23, 245–251 and 301–308 in CDK6.

Structure analysis. Proteins were superimposed on Cα atoms using OVRLAP[29] with the simple progression rule. Hydrogen bonds and van der Waals contacts were assigned with CONTACSYM[30]. The cutoff for hydrogen bonds and salt bridges was 3.4 Å and up to 4.11 Å for van der Waals contacts, depending on the atom type and using standard van der Waals radii. Buried surface areas were calculated with MS[31] and a 1.4 Å probe radius.

Coordinates. Coordinates have been deposited in the Protein Data Bank (accession code 1JOW).

Acknowledgments
We thank J. Brandsen for his exploratory work on protein expression and purification and E. Berry for helpful discussions. This work was supported by grants from NIH and DOE.

Correspondence should be addressed to U.S.G. *email: uschulze-gahmen@lbl.gov*

Received 16 August, 2001; accepted 18 December, 2001.

1. Sherr, C.J. *Cell* **73**, 1059–1065 (1993).
2. Sherr, C.J. *Cell* **79**, 551–555 (1994).
3. Pavletich, N.P. *J. Mol. Biol.* **287**, 821–828 (1999).
4. Hall, M. & Peters, G. *Adv. Cancer Res.* **68**, 67–108 (1996).
5. Sherr, C.J. *Science* **274**, 1672–1677 (1996).
6. Mittnacht, S. & Boshoff, C. *Rev. Med. Virol.* **10**, 175–184 (2000).
7. Jung, J.U., Stager, M. & Desrosiers, R.C. *Mol. Cell. Biol.* **14**, 7235–7244 (1994).
8. Li, M. *et al. J. Virol.* **71**, 1984–1991 (1997).
9. Godden-Kent, D. *et al. J. Virol.* **71**, 4193–4198 (1997).
10. Swanton, C. *et al. Nature* **390**, 184–187 (1997).
11. DeBondt, H.L. *et al. Nature* **363**, 595–602 (1993).
12. Jeffrey, D.P. *et al. Nature* **376**, 313–320 (1995).
13. Schulze-Gahmen, U., Jung, J.U. & Kim, S.-H. *Structure* **7**, 245–254 (1999).
14. Russo, A.A., Jeffrey, P.D. & Pavletich, N.P. *Nature Struct. Biol.* **3**, 696–700 (1996).
15. Card, G.L., Knowles, P., Laman, H., Jones, N. & McDonald, N.Q. *EMBO J.* **19**, 2877–2888 (2000).
16. Jeffrey, P.D., Tong, L. & Pavletich, N.P. *Genes Dev.* **14**, 3115–3125 (2000).
17. Russo, A.A., Tong, L., Lee, J.-O., Jeffrey, P.D. & Pavletich, N.P. *Nature* **395**, 237–243 (1998).
18. Brotherton, D.H. *et al. Nature* **395**, 244–250 (1998).
19. Brown, N.R., Nobel, M.E.M., Endicott, J.A. & Johnson, L.N. *Nature Cell Biol.* **1**, 438–443 (1999).
20. Hol, W.G.J., Van Duijnen, P.T. & Berendsen, H.J.C. *Nature* **273**, 443–446 (1978).
21. Kitagawa, M. *et al. EMBO J.* **15**, 7060–7069 (1996).
22. Ellis, M. *et al. EMBO J.* **18**, 644–653 (1999).
23. Russo, A.A., Jeffrey, P.D., Patten, A.K., Massague, J. & Pavletich, N.P. *Nature* **382**, 325–331 (1996).
24. Schulze-Gahmen, U. & Kim, S.-H. *Acta Crystallogr. D* **57**, 1287–1289 (2001).
25. Otwinski, Z.M., & Minor, W. *Methods Enzymol.* **276**, 307–326 (1997).
26. Collaborative Computational Project, Number 4 *Acta Crystallogr. D* **50**, 760–763 (1994).
27. Brünger, A.T. *et al. Acta Crystallogr. D* **54**, 905–921 (1998).
28. Jones, T.A., Zou, J.Y., Cowan, S.W. & Kjelgaard, M. *Acta Crystallogr. D* **47**, 110–119 (1991).
29. Rossman, M.G. & Argos, P.A. *J. Biol. Chem.* **250**, 7525–7532 (1975).
30. Sheriff, S., Hendrickson, W.A. & Smith, J.L. *J. Mol. Biol.* **197**, 273–296 (1987).
31. Connolly, M.L. *J. Appl. Crystallogr.* **16**, 548–558 (1983).
32. Thompson, J.D., Higgins, D.G. & Gibson, T.J. *Nucleic Acids Res.* **22**, 4673–4680 (1994).
33. Read, R.J. *Acta Crystallogr. A* **42**, 140–149 (1986).